Available online at www.sciencedirect.com
ScienceDirect
Journal of the European Ceramic Society 30 (2010) 2435–2441
www.elsevier.com/locate/jeurceramsoc

Boron-doped mullite derived from single-phase gels

Guimin Zhang [a,b], Zhengyi Fu [a,*], Yucheng Wang [a], Hao Wang [a], Weimin Wang [a], Jinyong Zhang [a], Soo Wohn Lee [c], Kochi Niihara [d]

[a] State Key Lab of Advanced Technology for Materials Synthesis and Processing, Wuhan University of Technology, Wuhan 430070, PR China
[b] Department of Chemistry, School of Sciences, Wuhan University of Technology, Wuhan 430070, PR China
[c] Department of Materials Engineering, SunMoon University, Asar, ChungNan 336-708, Republic of Korea
[d] Extreme Energy Density Research Institute, Nagoka University of Technology, 1603-1, Kamitomioka, Nagoba Niigata 940-2188, Japan

Received 29 October 2009; received in revised form 11 May 2010; accepted 18 May 2010

Abstract

Mullite with low dielectric constant and high transparency in infrared and microwave range has potential applications in communication industry. To improve the above properties of mullite, boron-doped mullite single-phase gels with a constant molar ratio of Al/Si = 3/1 and various B/Al ratios (B/Al = 0–0.4/3) were prepared in this study by slow hydrolysis of aluminum nitrate, boric acid and tetraethoxysilane. It was found that boron reduces the mullite formation temperature and suppresses spinel formation. The cell unit lattice parameters and cell volume in boron-doped mullite generally decrease with the increase of boron amount. The SEM observation shows that a small amount of boron reduces the grain sizes of mullite sintered bodies while a large amount of boron facilitates the formation of elongated grains and the amorphous glass phase. Boron decreases the transmittance of mullite ceramic and produces additional intensive absorption bond at 3.9 μm and also reduces the dielectric constants in the frequent range of 1 M–1 GHz.
© 2010 Elsevier Ltd. All rights reserved.

Keywords: Mullite; Sol–gel process; Optical properties; Dielectric properties

1. Introduction

Mullite ($3A1_2O_3{\cdot}2SiO_2$) has been recognized as an important structural and optical material due to its excellent high temperature strength, creep resistance, good chemical and thermal stability, low thermal expansion coefficient and infrared transparency.[1–4] Particularly, mullite with high transparency in infrared and microwave range could have special applications in communication industry where infrared and microwave could pass through mullite window without signal loss. The replacement of cation is an effective way to improve the property of mullite.[5–7] By the replacement of cation, dielectric constant of mullite can be decreased, and transparent mullite in infrared and microwave range can thus be fabricated because ceramic (e.g. mullite) with lower dielectric constant has better transparency property in microwave range. Existing study also showed low dielectric constant and optical transmittance of the fine-grained polycrystalline mullite have made it a good candidate for a host material as a solid-state laser activator.[8] The dielectric constant of material usually decreases with ionic polarizability. In all cations explored so far, the polarizability of B^{3+} ion is nearly the lowest. So B^{3+} ion is the potential candidate as replacement element for the reasons mentioned above. The influence of boron on the formation temperature and the microstructure of mullite were investigated by some scholars. In diphasic gels, boron is known to enhance the transformation kinetics in mullite.[9,10] Hong et al. found the mullite transformation temperature was decreased by 150 °C in 5 wt% B_2O_3-doped diphasic gels and anisotropic grain growth was enhanced.[11] They believed this (i.e. the enhanced transformation kinetics in boria-doped samples) was because the faster diffusion in the lower viscosity boria-containing glasses,[12] not firstly forming aluminum borate, $9Al_2O_3{\cdot}2B_2O_3$, had worked as an epitaxial substrate for mullite nucleation and growth as previously reported by Sowman.[13] Anisotropic grain growth is a result of liquid phase occurring in sintering process. Griesser et al. measured the lattice parameters of boron-doped mullite powder.[14] The results indicated a large amount of boron were incorporated into mullite structure

* Corresponding author. Tel.: +86 027 87662983; fax: +86 027 87879468.
E-mail address: zyfu@whut.edu.cn (Z.Y. Fu).

0955-2219/$ – see front matter © 2010 Elsevier Ltd. All rights reserved.
doi:10.1016/j.jeurceramsoc.2010.05.017

Table 1
The boria amount in mullite Gels and corresponding boron-doped mullite lattice parameters.

Sample	B/Al (molar ratio)	Mass content of boria (wt%)	Mullite lattice parameter			
			a (nm)	*b* (nm)	*c* (nm)	*V* (nm^3)
B000	0	0	0.75494(11)	0.76939(15)	0.28852(5)	0.167583
B005	0.05/3	0.81	0.75412(18)	0.76957(18)	0.28819(5)	0.167252
B010	0.1/3	1.61	0.75529(18)	0.76977(20)	0.28788(6)	0.167376
B015	0.15/3	2.39	0.75526(17)	0.76934(15)	0.28753(4)	0.167069
B020	0.2/3	3.16	0.75417(22)	0.76957(24)	0.28696(7)	0.166544
B030	0.3/3	4.67	0.75447(25)	0.76910(29)	0.28688(12)	0.1664679
B040	0.4/3	6.14	0.75337(22)	0.76811(23)	0.28565(7)	0.1652979

(up to about 20 mol% B_2O_3 depending on the bulk composition of the starting materials). However, in monophasic gels, very little information is reported about the influence of boron on mullite formation kinetics and its physical properties. In the present investigation, the sol–gel method was adopted to achieve monophasic boron-doped mullite precursor. The effects of the B_2O_3 amount on mullite formation temperature, sinterability, microstructure and physical properties were investigated. The methods of boron being incorporated into the mullite and the doping quantity were also explored.

2. Experimental

2.1. Sample preparation

The boron-doped mullite powders were prepared by sol–gel method. Aluminum nitrate-nonahydrate (ANN), boric acid and tetraethoxysilane (TEOS) were used as starting materials. ANN and boric acid were firstly dissolved in absolute ethanol and stirred at 60 °C for 24 h under reflux. The molar ratio of Al/Si was constant 3/1 and the molar ratio of Al/B varied from 3/0.05 to 3/0.4. The stoichiometric amount of TEOS dissolved in absolute ethanol in advance was slowly dropped into the above solution. The resulted mixture solution was stirred under reflux at 60 °C for 4 days and then aged at the same temperature for around 5 days without being stirred. Finally, physical gels were obtained. The gels were dried at 110 °C for 2 days, then crushed and ground to powders. The precursor powder was calcined at 1000 and 1400 °C for 4 h at the heating rate of 10 °C/min for sintering and measuring lattice parameters, respectively. In the present study, six types of precursors with different amounts of boron were named as B000, B005, B010, B020, B030, B040, respectively, according to the molar ratio of B/Al. For example, the sample with the molar ratio of B/Al being equal to 0.05/3 was named as B005. The compositions of these samples were listed in Table 1.

The calcined powder was then poured into a graphite mold (inner diameter of 15 mm, outer diameter of 40 mm) and sintered at 1450 °C for 10 min by Spark Plasma Sintering (SPS) (Model SPS-3.20MK II, Japan) at a heating rate of 100 °C/min in vacuum. A pressure of 30 MPa was applied onto the samples from the beginning of the sintering process. The thickness of sintered specimens is about 3 mm.

2.2. Characterization methods

The mullite formation temperature was determined by differential thermal analysis (DTA) at 10 °C/min in air (Model STA-449C, Netzsch, German). X-ray diffraction analysis (Model D/max-RB, Rigaku, Japan) was performed between 10° and 90° (2θ) using a graphite monochromatic Cu Kα radiation, with a step of 0.02° and a scanning rate of 0.5°/min. About thirty reflections were collected for determining the lattice constants with silicon being an internal standard. Diffraction peaks were indexed with (MDI) Jade 5 software. Lattice parameters were calculated with the Unitcell program. KBr pellets were prepared for the IR powder measurements. The sintered samples were sliced (0.94 mm in thickness) and polished for infrared transmittance testing. Infrared absorption spectra (AVATAR370, Nicolet, USA) were obtained within the range of 4000–400 cm^{-1}. The microstructures of sintered samples were examined by scanning electron microscopy (S-3400, Hitachi, Japan) equipped with energy dispersive X-ray (EDX) analysis. The polished samples were thermally etched at 100 °C below the sintering temperature for SEM and chemically etched with NaOH and HF solutions for EDX analysis. The relative dielectric constants (ε_r) were measured within the range of 1 MHz to 1 GHz at room temperature, using an HP 4291B alternating current impedance analyzer (HP/Agilent).

3. Results and discussion

3.1. Powder characterization

DTA patterns of mullite gels containing 0–4.7 wt% B_2O_3 are shown in Fig. 1. The DTA pattern of pure mullite gels contains an exothermic peak at 989.7 °C, which is associated with mullite formation, and a small broad exothermic peak at 1304.3 °C, which is due to the phase change from spinel to mullite. The DTA patterns of all boron-doped mullite gels display only one exothermic peak above 900 °C. This indicates that boron-doped mullite precursors are single-phase gels which are directly transformed into mullite from amorphous phase without intermedia phase spinel or other aluminum borate. It can be observed that the crystallization temperature decreases with the increase of B_2O_3 amount, as shown in Fig. 2. Mullite gels containing 4.7 wt% B_2O_3 crystallized at 948.6 °C, which is 41.1 °C lower than that

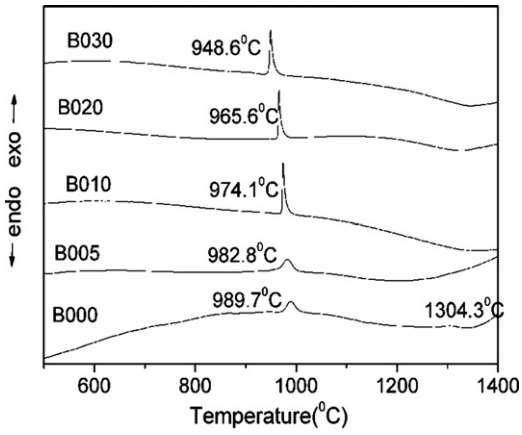

Fig. 1. DTA pattern of pure mullite gel and boron-doped mullite gel at a heating rate of 10 °C/min in air.

of pure mullite gels. Hong et al. reported that formation temperature of mullite with 5 wt% boria decreased by 150 °C compared to that of the undoped diphasic gels. In the present experiments, boron does not have such a great effect on the transformation kinetics in the single-phase gels as in the diphasic gels.

The XRD patterns of different boron-doped samples heat-treated at 1000 and 1400 °C are shown in Fig. 3(a) and (b), respectively. All samples transformed into mullite when they were heat-treated at 1000 °C for 4 h. In sample B000, a small amount of spinel coexisted with mullite. The result is consistent with the DTA result shown in Fig. 1 which indicates that the pure mullite precursor is a mixture composed of a large amount of single-phase and a small amount of diphasic gel (the spinel at about 980 °C). In all boron-doped samples, spinel cannot be detected. Based on the analysis from XRD and DTA date, it can be concluded that boron facilitates the direct transformation of precursor into mullite and suppresses the formation of spinel. The influence of boron on crystallization of Al_2O_3–SiO_2 gels is different from that of chromium and titanium. In Cr-doped and Ti-doped single-phase gels, two-step phase separation was proposed.[15,16] The first-step is the separation into alumina-rich and silica-rich phases. The second step is the clustering of alumina-rich phase. As the content of alumina in clusters exceeds the upper value of its solubility limit in mullite, the

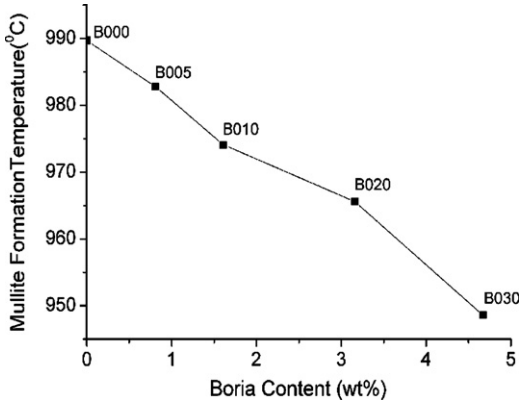

Fig. 2. Relationship between mullite formation temperature and boron amount.

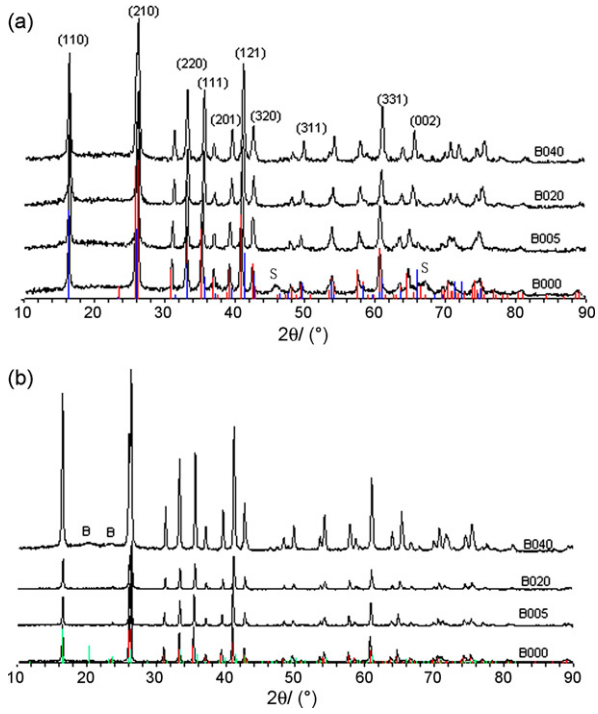

Fig. 3. XRD pattern of different amount of boria sample calcined at (a) 1000 °C, (b) 1400 °C (B is aluminum borate, S is spinel. The red, blue, and green lines represent the diffraction peaks of mullite (card #15-0776), $Al_4B_2O_9$ (card #47-0319) and $Al_{18}B_4O_{33}$ (card #32-0003), respectively). (For interpretation of the references to colour in this figure legend, the reader is referred to the web version of the article.)

crystallization of spinel from the same clusters initiates. Adding chromium and titanium stimulates the formation of clusters, leading to the crystallization of spinel in nonisothermal treatment. However, in the present study, the second-step phase separation is suppressed in boron-doped single-phase gels, thus leading to the disappearance of the spinel phase. As a result, a type of relatively highly chemically homogenous gels is attained in the system of the present study.

When diffraction peaks of boron-doped mullite and that of pure mullite (card #15-0776) are compared, it is observed that some diffraction peaks of boron-doped mullite shift. It is clear that the two pairs of peaks at the 2θ of about 71° and 75° overlap in pure mullite but split in boron-doped mullite. For samples calcined at 1000 °C, no additional diffraction peaks were found in all boron-doped mullite except that some diffraction peaks have gradually shift to the corresponding positions of aluminum borate $Al_4B_2O_9$ crystals (card # 47-0319). It should be noted that $Al_4B_2O_9$ has the same orthorhombic crystal structure as mullite and their lattice parameters are also close to each other, with $a = 7.617$, $b = 7.617$, $c = 2.827$ for $Al_4B_2O_9$ and $a = 7.545$, $b = 7.689$, $c = 2.884$ for mullite. For crystal planes (1 1 0), (2 1 0), (2 2 0) and so on, the d-spaces of $Al_4B_2O_9$ are nearly equal to that of mullite. In boron-doped mullite, the diffraction peaks of the above crystal planes do not shift. While for crystal planes (1 1 1), (2 0 1), (3 3 1), (0 0 2) and so on, the d-space differences between $Al_4B_2O_9$ and mullite are larger than 0.002 nm. In boron-doped mullite, the shift of the diffraction peaks of these crystal planes

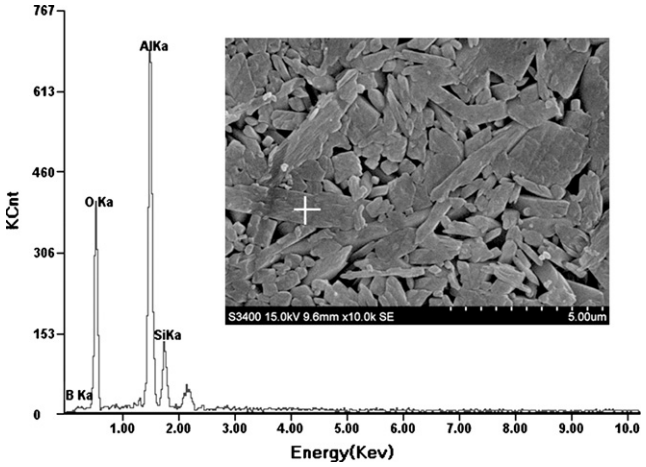

Fig. 4. SEM micrograph and EDX spectrum of the sample B040 (the sample was sintered at 1450 °C for 10 min by SPS and etched by NaOH and HF solutions).

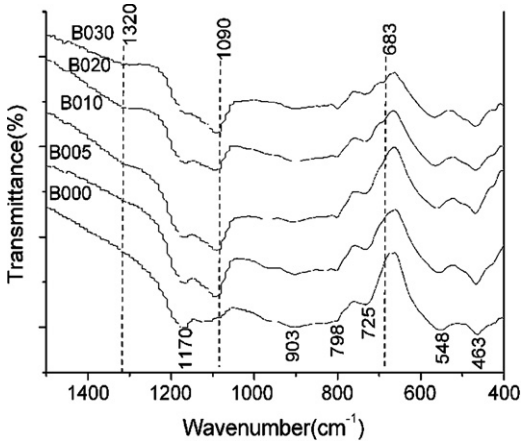

Fig. 5. IR absorption spectra of pure mullite and boron-doped mullite powder calcined at 1400 °C for 4 h.

increases with increasing boron amount. Even using a slowly scanning rate of 0.5°/min, no split can be observed for these shifted peaks. This indicates the boron-doped mullite is not a simple mixture of pure mullite and $Al_4B_2O_9$, but a solid solution which includes some units with the same structure as mullite and $Al_4B_2O_9$. For the samples calcined at 1400 °C, the XRD pattern of sample B040 shows two additional diffractions with low intensity at the 2θ of about 20.3° and 23.7° besides that some diffraction peaks have gradually shifted to the diffraction line of $Al_{18}B_4O_{33}$ (card #32-0003) with the increase of boron amount. Based on the above information, we identified the impurity phase as mullite-type $Al_{18}B_4O_{33}$, whose diffraction lines are partially overlapped with that of mullite due to the similar crystal structure (orthorhombic) and lattice parameters (i.e. $a = 7.687$, $b = 15.01$, $c = 5.664$, where b and c in $Al_{18}B_4O_{33}$ are nearly twice as much as that in mullite) with mullite. Although the shifted peaks do not split, the shift distances of samples calcined at 1400 °C are smaller than that of the samples calcined at 1000 °C. This means that not all B_2O_3 has entered mullite lattice structure at 1400 °C, but that only part of them has formed aluminum borate which coexists with mullite. Boron-doped samples are always in amorphous state before they transform into mullite (the XRD patterns are not shown here). Therefore aluminum borate is not an epitaxial substrate for mullite nucleation and growth. The presence of boron decreases the viscosity of the amorphous SiO_2-rich phase. The low viscosity promotes atomic diffusion, mullite nucleation and growth. The result is consistent with the results of Hildmann's[9] and Hong's[10] studies.

Table 1 shows the relationship between boron amount and lattice parameters. From this table, it is clear that lattice parameter c and unit cell volume decrease continuously with the increase of boron amount although small variation exists. The decrease in the lattice parameter c and unit cell volume is a strong evidence that boron is incorporated into mullite structure. The conclusion that the boron is in solid solution is also supported by the EDX result shown in Fig. 4 which clearly indicates boron element exists in the chemically etched mullite crystals. Griesser et al.[14] believed that boron is substituted for silicon in tetrahedral sites to enter mullite structure, and the maximum amount of solid solution is up to about 20 mol% B_2O_3 in 60 mol% Al_2O_3. Boron can enter tetrahedral sites of mullite structure due to its inherent property; nevertheless, the present study indicates B_2O_3 in precursor is also favorable to react with Al_2O_3 to form $Al_{18}B_4O_{33}$ above 1400 °C. So the 20 mol% B_2O_3-containing mullite cannot be made. The substitution of B^{3+} for Si^{4+} would possibly lead to the simultaneous occurrence of the following events to preserve electroneutrality: oxygen anionic vacancies, boron cationic interstice and replacement of tetrahedral Al^{3+} with Si^{4+}. However, these simultaneous events cannot change lattice parameters as significantly as the substitution of B^{3+} for Si^{4+}. The radius of B^{3+} ion (0.02 nm) is smaller than that of Si^{4+} ion (0.041 nm). So the lattice parameter and volume generally decrease with increasing boron amount and the variation in the c-axis is more obvious than in the a-axis and b-axis. Fluctuations in the lattice parameters a and b are probably caused by experimental errors given that the magnitude of these fluctuations is very small.

IR spectra of different amount of boron mullite in the 1500–400 cm^{-1} region are shown in Fig. 5. It should be noted that in Fig. 5, only several representative IR absorption peaks are presented to show the general features of all samples. The peaks at around 1170 and 903 cm^{-1} are assigned to the in-plane and out-of-plane stretching vibrations of Al–O in AlO_4, respectively. The peaks at 725, 548 and 463 cm^{-1} correspond to the bending vibration of Al–O in AlO_4, AlO_6 and Si–O in SiO_4, respectively. The band located at around 798 cm^{-1} is assigned to the stretching vibration of Al–O in AlO_6.[17,18] Different from the pure mullite, in all boron-doped mullite samples, a new absorption peak appears at 1090 cm^{-1} which is attributed to the stretching vibration of BO_4 tetragon. The intensity of the peak is a constant which is not affected by boron amount. As boron amount increases, a broad bond at around 1320 cm^{-1} and a weak shoulder peak at 683 cm^{-1} begin to appear in samples B010 and B020, which are attributed to the stretching vibration of BO_3 triangle and the bending vibration of BO_3 triangle[14] respectively. The intensities of the two peaks increase with the increase of boron amount.

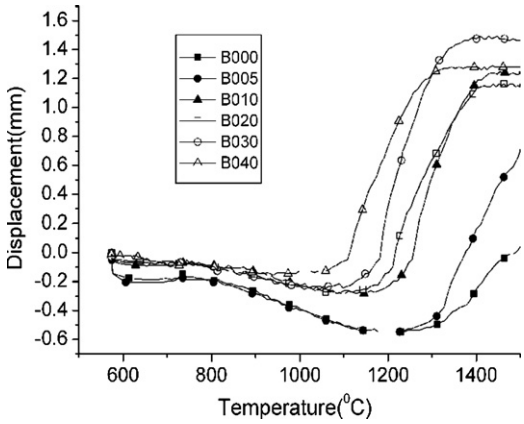

Fig. 6. Relationship between displacement and sintering temperature for samples with different amount of boria.

3.2. Sintering behavior and microstructure

Fig. 6 shows the relationship between displacement and sintering temperature for samples with different amount of boron in the sintering process. The positive and negative values of displacement mean the shrinkage and expansion of samples, respectively. The shrinkage during sintering indicates the sample is being densified. Pure mullite densification takes place between 1240 and 1530 °C (only the range below 1500 °C is shown in Fig. 6). The densification temperature of sample B005 is almost the same as pure mullite. This is expected because B005 has only small amount of boron. For sample B010, B020, B030, B040, the densification process occurs at a temperature between 1150 and 1450, 1090 and 1440, 1060 and 1410, 940 and 1350 °C, respectively. It is clear that increasing boron amount reduces the densification temperature and extends the temperature range of the sintering process. In the sintering process of mullite derived from single phase gel by SPS, although the powder has already been transformed into mullite before sintering, the viscous flow sintering mechanism still plays a significant role due to the existence of a small amount of amorphous phase.[19] Boria–silica glass phase has a much lower viscosity compared to pure vitreous silica (e.g. $10^{5.1}$ Pa s for 28 wt% boria–72 wt% silica versus $10^{10.2}$ Pa s for silica at 1300 °C).[20] As a result, increasing boron content reduces the densification temperature.

Fig. 7 shows the microstructures of pure and boron-doped mullites dense bodies sintered at 1450 °C for 10 min by SPS. The microstructure of pure mullite (i.e. B000) consists of very few elongated grains and a large number of fine equiaxial grains with an average size of 0.5 μm. In sample B005, the diameter of equiaxed gain is smaller and the length of elongated grain is longer. It is clear that both the number and length of elongated grains increase with the increase of boron amount. In sample B020, the number of elongated grains is so large that they impinge upon one another and form a three-dimensional, interpenetrating microstructure. The glass phase on the grain boundaries and the triple junction regions also increase. As a result, the grain boundaries become broader. This fact further indicates that a large amount of boria coexists with alumina and silica glass in the amorphous state and only part of boron enters into mullite crystal structure.

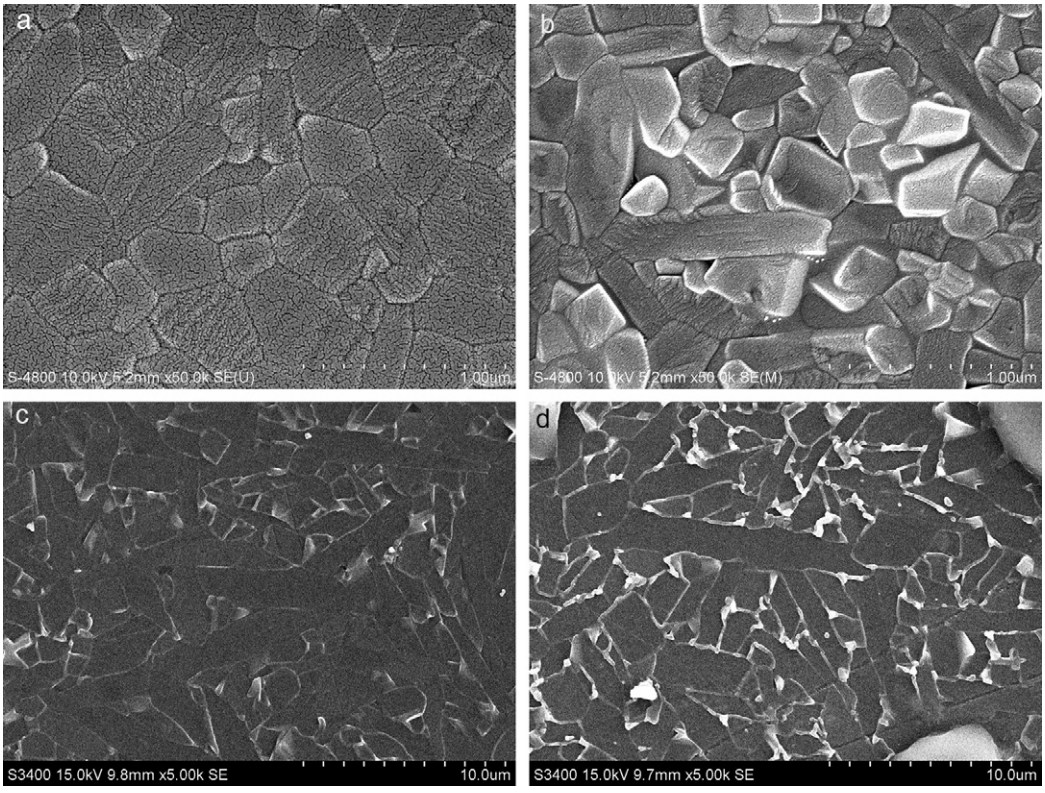

Fig. 7. SEM micrographs of pure and boron-doped mullite sintered at 1450 °C for 10 min by SPS (a) pure mullite; (b) sample B005; (c) sample B020; (d) sample B040.

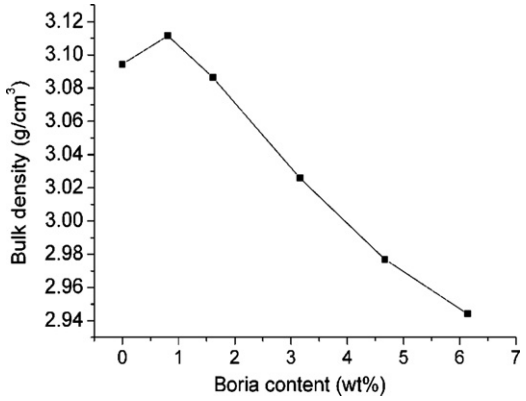

Fig. 8. Dependence of mullite bulk density on the weight percentage of boria content (the samples were sintered at 1450 °C for 10 min by SPS).

Fig. 8 shows the relationship between the bulk density of boron-doped mullite and boria amount. All the samples were sintered at 1450 °C for 10 min by SPS. It can be seen that increasing boron amount reduces the bulk density. Two factors contribute to the density reduction. One factor is that the boron weight less than silicon. The other factor is that the boron amount increases the sample volume during sintering process as shown in Fig. 6.

3.3. Properties

Fig. 9 shows the appearances and spectral transmittances of pure and boron-doped mullites sintered at 1450 °C for 10 min by SPS. The slice samples were placed on top of a newspaper. The letters under the pure mullite ceramic slice are clearly legible, and the slice in color is inhomogenous. The letters under sample B005 can be vaguely seen and the sample B010 is almost opaque. However the color in both sample B005 and B010 is homogenous. As shown in Fig. 9(b), boron decreases the transmittance of mullite in IR wavelength range and produces additional intensive absorption band centered at about 3.9 μm due to the vibration of B–O bond. Furthermore, it makes the absorption at 4.3 μm more intensive. When boron amount is above 1.61 wt%, mullite becomes completely opaque. This is because a large amount of boron-doped glass phase has congregated in grain boundaries and triple junction regions as impurity. Furthermore, the number of elongated grains also increases with the increase of boron amount.

Fig. 10 shows the relationship between the light wave frequency and the dielectric constants of pure and boron-doped mullite sintered at 1450 °C for 10 min. The data shows increasing boron amount reduces the dielectric constant. For instance, at 1 MHz, the dielectric constant of sample drops from 7.01 to 6.36 when boron amount increases from 0 to 6.14%. The decrease in dielectric constant is possibly related to the increasing micro-pores in sintered bodies. However, it can be seen from Fig. 7 that all samples have nearly the same porosity. Thus, the decrease in dielectric constant is due to the substitution of B^{3+} for Si^{4+}. Our data have shown that the B^{3+} substitution decreases the volume of unit cell, and thus reduces the free space for atom motion. This leads to the decrease of ionic polarizability which is the key factor affecting the dielectric constant. Furthermore, the

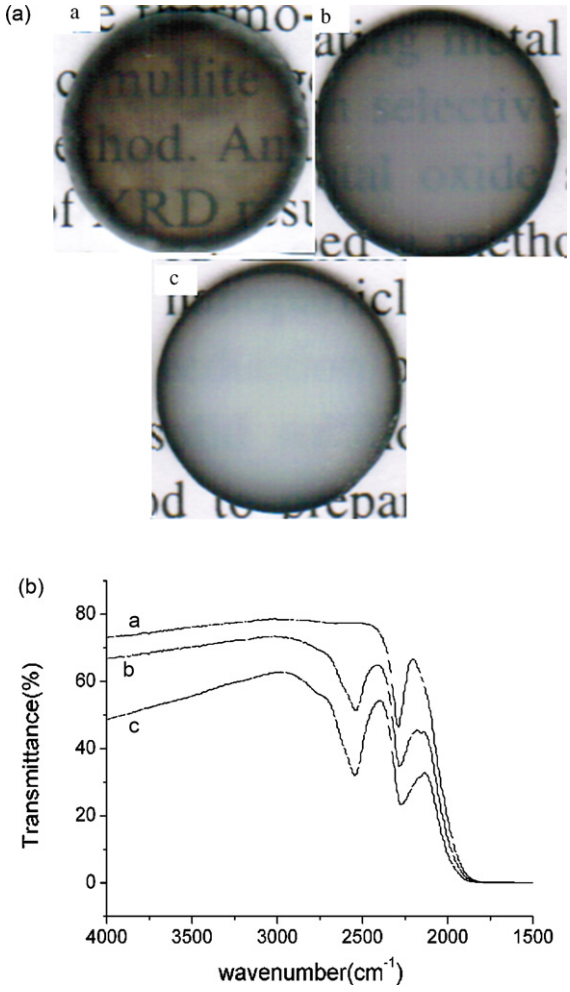

Fig. 9. Appearance and spectral transmittance in IR wavelength range of pure and boron-doped mullite ceramic sintered at 1450 °C for 10 min by SPS: (a) appearance; (b) spectral transmittance in IR wavelength range (the thickness of ceramic slice is 0.94 mm. a: pure mullite; b: sample B005; c: sample B010).

polarizability of B^{3+} is lower than that of Si^{4+}. Thus the substitution of B^{3+} for Si^{4+} decreases the total polarization capability and leads to the lower dielectric constant of in boron-doped mullite.

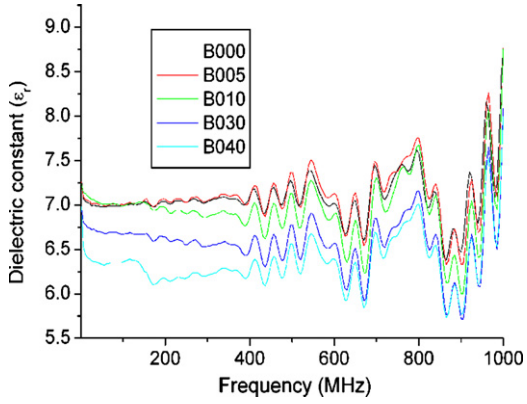

Fig. 10. Relationship between light wave frequency and dielectric constants of mullite ceramics with different amount of boron (all samples were sintered at 1450 °C for 10 min by SPS).

4. Conclusions

For boron-doped mullite, boron reduces the glass phase viscosity and enhances atomic diffusion rate, and thus decreases both mullite formation temperature and densification temperature. The experimental evidences presented in this study have shown that boron is incorporated into mullite structure and decreases both the lattice parameters and cell volume. A small amount of boron can reduce mullite grain sizes and enhance the color homogeneity, but large amount of boron can make mullite lose transparency because boron-doped grass phase congregates in grain boundaries and triple junction regions and large amount of impinged elongated grains form. Boron-doped mullite generates an additional intensive absorption bond at 3.9 μm resulting from the vibration of B–O bond. The dielectric constants of boron-doped mullite ceramics generally decrease with the increase of boron content in the frequent range of 1 M–1 GHz.

Acknowledgements

The authors thank the National Nature Science Foundation of China (50772081, 50821140308) and the Ministry of Education of China (PCSIRT0644) for financial support to the research.

References

1. Schneider H, Schreuer J, Hildmanna B. Structure and properties of mullite—a review. *J Eur Ceram Soc* 2008;**28**:329–44.
2. Aksay, IIhan A, Dabbs, Daniel M, Sarikaya M. Mullite for structural, electronic, and optical applications. *J Am Ceram Soc* 1991;**74**:2343–58.
3. Prochazka S, Klug FJ. Infrared transparent mullite ceramic. *J Am Ceram Soc* 1983;**66**:874–80.
4. Schneider H, Schmucker M, Ikeda K, Kaysser WA. Optically translucent mullite ceramics. *J Am Ceram Soc* 1993;**76**:2912–4.
5. Murthy MK, Hummel FA. X-ray study of the solid solution of TiO_2, Fe_2O_3, and Cr_2O_3 in mullite ($3A1_2O_3{\cdot}2SiO_2$). *J Am Ceram Soc* 1960;**43**(5):267–73.
6. Kong LB, Zhang TS, Ma J, Boey F. Some main group oxides on mullite phase formation and microstructure evolution. *J Alloy Compd* 2003;**359**:292–9.
7. Parmentier J, Vilminot S. Influence of transition metal oxides on sol–gel mullite crystallization. *J Alloy Compd* 1998;**264**:136–41.
8. Fang Y, Roy R, Agrawal DK, Roy DM. Transparent mullite ceramics from diphasic aerogels by microwave and conventional processings. *Mater Lett* 1996;**28**:11–5.
9. Hildmann BO, Schneider H, Schmiicker M. High temperature behaviour of polycrystalline aluminosilicate fibres with mullite bulk composition. II. Kinetics of mullite formation. *J Eur Ceram Soc* 1996;**16**: 287–92.
10. Hong SH, Messing GL. Mullite transformation kinetics in P_2O_5-, TiO_2-, and B_2O_3-doped aluminosilicate gels. *J Am Ceram Soc* 1997;**80**(6):1551–9.
11. Hong SH, Cermignani W, Messing GL. Anisotropic grain growth in seeded and B_2O_3-doped diphasic mullite gels. *J Eur Ceram Soc* 1996;**16**:133–41.
12. Hong SH, Messing GL. Anisotropic grain growth in boria-doped diphasic mullite gels. *J Eur Ceram Soc* 1999;**19**:521–6.
13. Sowman HG. Alumina–boria–silica ceramic fibers from the sol–gel process. In: Klein LC, editor. *Sol–gel technoloy for thin films, fibers, performs, electronics, and specialty shapes*. Park Ridge, NJ: Noyes; 1988. pp. 162–82.
14. Griesser KJ, Beran1 A, Voll1 D, Schneider H. Boron incorporation into mullite. *Mineral Petrol* 2008;**92**:309–20.
15. Nass R, Tkalcec E, Ivankovic H. Single-phase mullite gels doped with chromium. *J Am Ceram Soc* 1995;**78**(11):3097–106.
16. Sola ER, Estevan F, Alarcon J. Low-temperature Ti-containing 3:2 and 2:1 mullite nanocrystals from single-phase gels. *J Eur Ceram Soc* 2007;**27**:2655–63.
17. Mackenzie KJD. Infrared kinetic study of high-temperature reactions of synthetic kaolinite. *J Am Ceram Soc* 1969;**52**(12):635–7.
18. Voll D, Angerer P, Berana A, Schneider H. A new assignment of IR vibrational modes in mullite. *Vibrat Spectrosc* 2002;**30**:237–43.
19. Zhang GM, Wang YC, Fu ZY, Wang H, Wang WM, Zhang JY, et al. Transparent mullite ceramic from single-phase gel by Spark Plasma Sintering. *J Eur Ceram Soc* 2009;**29**:2705–11.
20. Bansal NP, Doremus RH. *Handbook of glass properties*. New York: Academic Press; 1986.